

Preclinical Development

Glycolytic Inhibition Alters Anaplastic Thyroid Carcinoma Tumor Metabolism and Improves Response to Conventional Chemotherapy and RadiationVlad C. Sandulache^{1,2}, Heath D. Skinner³, Yuan Wang², Yunyun Chen², Cristina T. Dodge², Thomas J. Ow², James A. Bankson⁴, Jeffrey N. Myers², and Stephen Y. Lai^{2,5}**Abstract**

Anaplastic thyroid carcinoma (ATC) accounts for more than 50% of thyroid cancer mortality and is generally refractory to conventional treatment. On the basis of recent studies, we hypothesized that ATC metabolism can be targeted to improve response to chemoradiotherapy. Eight established and authenticated ATC cell lines were sequenced at 140 sites contained within 26 commonly mutated genes to identify novel potential therapeutic targets. Cellular proliferation, energy, and reducing potential stores were measured under conditions of specific nutrient deprivation. Tumor metabolism was evaluated using hyperpolarized ¹³C MRI in a murine orthotopic xenograft model of ATC. Sensitivity to chemotherapeutic agents and radiation (XRT) was assayed using cytotoxicity assays. We identified mutations in *BRAF*, *NRAS*, and *KIT* but failed to identify generalized novel targets for therapeutic intervention. ATC cell lines exhibited a mesenchymal phenotype and generalized dependence on glucose for energy, reducing potential and survival. Glycolytic inhibition using 2-deoxyglucose (2-DG) sensitized ATC cells to conventional chemotherapy and external beam radiation. *In vivo*, 2-DG induced a transient, but significant reduction in ATC metabolic activity. Generalized dependence of ATC cells on glucose catabolism makes them susceptible to the sensitizing effects of 2-DG for radiation therapy and chemotherapy. Under *in vivo* conditions, 2-DG can inhibit ATC metabolism. However, the modest magnitude and transient nature of this effect suggest the need for antimetabolic agents with more favorable pharmacodynamics to achieve therapeutic effects. *Mol Cancer Ther*; 11(6); 1373–80. ©2012 AACR.

Introduction

Anaplastic thyroid carcinoma (ATC) is a rare and aggressive cancer of the thyroid with extremely poor prognosis. Although ATC only comprises 1.7% of all thyroid cancers in the United States, it accounts for more than 50% of thyroid carcinoma-related deaths (1–3). Cellular dedifferentiation, locoregional invasion and distant metastasis are characteristic features of ATC (2). Despite the use of multimodality treatment combining surgery, external beam radiation, and chemotherapy, the median survival rate (5 months) has improved little over the last few decades. Poor outcomes associated with ATC can be

attributed in part to tumor cell resistance to both conventional and targeted chemotherapeutic strategies. Treatment failure and high rates of locoregional and distant metastasis make the development of effective chemotherapeutic agents an urgent necessity.

One hallmark of rapidly proliferating tumor cells is the shift from mitochondrial respiration to aerobic glycolysis (Warburg effect; ref. 4). Although aerobic glycolysis is inefficient from an energetic perspective, it can fulfill the biomass requirements associated with rapid proliferation (5). The distinct metabolism of tumor cells makes targeting of metabolic pathways a promising approach for therapeutic interventions. Metabolic agents targeted toward glucose catabolism [2-deoxyglucose (2-DG), lonidamine, and bromopyruvate], lactate transport (MCT inhibitors), mitochondrial respiration (metformin), and generalized protein synthesis (mTOR inhibitors) have been described, with varied effectiveness in a variety of solid tumors (6–13).

The metabolic activity of ATC remains poorly understood. However, indirect evidence suggests that, like other solid tumors, ATC exhibits high rates of glucose uptake and catabolism as indicated by overexpression of glucose transporters and increased ¹⁸F-fluoro-2-deoxyglucose (FDG)-positron emission tomography (PET) avidity (14, 15). Using established experimental paradigms, we

Authors' Affiliations: ¹Bobby R. Alford Department of Otolaryngology–Head and Neck Surgery, Baylor College of Medicine; and Departments of ²Head and Neck Surgery, ³Radiation Oncology, ⁴Imaging Physics, ⁵Cellular and Molecular Oncology, The University of Texas MD Anderson Cancer Center, Houston, Texas

Note: Supplementary data for this article are available at Molecular Cancer Therapeutics Online (<http://mct.aacrjournals.org/>).

Corresponding Author: Stephen Y. Lai, Departments of Head and Neck Surgery, Cellular and Molecular Oncology, The University of Texas MD Anderson Cancer Center, Houston, TX 77030. Phone: 713-792-6528; Fax: 713-794-4662; E-mail: sylai@mdanderson.org

doi: 10.1158/1535-7163.MCT-12-0041

©2012 American Association for Cancer Research.

sought to evaluate the metabolic profile of a comprehensive panel of ATC cell lines to determine optimal metabolic targeting strategies aimed at improving the effectiveness of conventional chemotherapeutic agents and external beam radiation. We further assessed the potential of metabolic targeting *in vivo* using an orthotopic ATC xenograft model and hyperpolarized ^{13}C MRI.

Materials and Methods

Cells

A total of 8 previously isolated and described ATC cell lines were used for this study. Cell lines were obtained from an established cell bank in the laboratory of Dr. Jeffrey N. Myers (University of Texas MD Anderson Cancer Center, Houston, TX) under approved institutional protocols. All cell lines were tested and authenticated using short-tandem repeat analysis within 6 months of use for the current project (16). Cells were maintained in either RPMI of MEM growth media supplemented with glutamine, pyruvate, penicillin/streptomycin, and 10% FBS. For proliferation and survival experiments, a baseline growth profile was obtained in Dulbecco's modified Eagle's medium containing 25 mmol/L D-glucose (GLC), and 4 mmol/L glutamine (GLN) to standardize conditions across cell lines. Cell phenotypes were further established using a combination of bright field imaging (standard growth conditions), immune-fluorescence, and Western blotting for expression of E-cadherin (BD Biosciences) and vimentin (Dako Cytomation). Sequencing analysis of 140 mutational hot spots in 26 genes was carried out as previously described (Supplementary Table S1; ref. 17).

Chemicals

2-Deoxyglucose and glutamine were purchased from Sigma-Aldrich. D-Glucose was purchased from ICN Biomedical. Cisplatin was obtained from APP Pharmaceuticals.

Metabolic studies

Intracellular ATP levels and cellular reducing potential were measured as previously described (18, 19). Proliferation and starvation experiments were carried out for 24 to 72 hours in media supplemented with glucose and glutamine. At the end of the experimental period, relative cell number was ascertained using total DNA content as a surrogate for cell number.

Cytotoxicity studies

Drug and XRT toxicity was assayed using clonogenic assays. ATC cells were irradiated using a high-dose rate ^{137}Cs unit (4.5 Gy/min) to the indicated dose. Cells were incubated with drugs of interest for 24 hours, allowed to recover for 10 to 14 days, then fixed and stained using a 1% formalin/crystal violet solution. Colonies were counted and surviving fractions were determined based upon the plating efficiency of the nonirradiated control group.

Orthotopic ATC tumors

Male athymic nude mice (8–12 weeks) were purchased from the National Cancer Institute (Bethesda, MD), maintained in a pathogen-free facility and fed irradiated mouse chow and autoclaved, reverse osmosis-treated water. The animal facility was approved by the American Association for the Accreditation of Laboratory Animal Care and met all current regulations and standards of the U.S. Department of Agriculture, U.S. Department of Health and Human Services, and the NIH. All procedures were approved by the Institutional Animal Care and Use Committee of The University of Texas MD Anderson Cancer Center. U-HTH83 luciferase expressing cells (2.5×10^5 per mouse) were injected into the right thyroid lobe under direct visualization as previously described (20). Control and 2-DG-treated (500 mg/kg administered intraperitoneal) thyroid tumors were imaged at 2 and 24 hours posttreatment. Following completion of imaging experiments, all animals were sacrificed and tumors were harvested for histologic evaluation.

Preparation of hyperpolarized [$1\text{-}^{13}\text{C}$]Pyruvate

An amount of 20 μL of [$1\text{-}^{13}\text{C}$]pyruvic acid (Isotec) doped with 15 mmol/L Ox63 polarizing radical (GE Healthcare) and 1.5 mmol/L ProHance (Bracco) was polarized using a HyperSense dynamic nuclear polarization (DNP) system (Oxford Instruments). The polarizing target was frozen to approximately 1.4 K in a 3.35T magnetic field and irradiated at 94.136 GHz for 45 to 60 minutes (21, 22). Once the solid-state polarization level reached a plateau, the preparation was dissolved in 4 mL of a heated (180°C) solution containing 80 mmol/L NaOH and 50 mmol/L NaCl, then flushed into a vessel from which 200 μL was drawn for injection. The final solution contained 80 mmol/L pyruvate with a nominal pH of 7.6 and temperature of 37°C.

MRI and dynamic spectroscopy

All hyperpolarized tracer data was acquired at 7T using a Biospec USR7030 system and B-GA12 imaging gradients (Bruker Biospin Corp). Anesthesia was induced and maintained using 0.5% to 5% isoflurane in oxygen. Animals were placed head first and supine on a sliding bed system. A surface coil (20 mm outer diameter) that was tuned for ^{13}C was placed over the thyroid. Anatomic imaging was done using the ^1H channel of a dual-tuned, actively decoupled $^1\text{H}/^{13}\text{C}$ volume resonator (72 mm ID; Bruker Biospin Corp). Animal positioning was confirmed using a 3-plane fast low-angle shot (FLASH) gradient-echo sequence (TE = 3.6 milliseconds, TR = 100 milliseconds) and the location of the tumor was observed in RARE T2-weighted axial and coronal spin-echo images (TE = 50 milliseconds, TR = 2,500 milliseconds, with echo train length of 8, 4 cm \times 3 cm FOV encoded over a 256 \times 192 matrix, and 1-mm slice thickness). For ^{13}C measurements, signal was excited using the ^{13}C channel of the dual-tuned resonator and detected using the surface coil. Dynamic spectra were acquired using a slice-selective

pulse-acquire sequence (SW = 5,000 Hz over 2,048 points, 10 degree excitation and 8-mm slice thickness) that was repeated every 2 seconds for 3 minutes beginning just before injection of 200 μ L of 80 mmol/L hyperpolarized pyruvate solution via tail vein catheter. Spectra were phase adjusted, and the area of the pyruvate and lactate spectral peaks was integrated to yield a time-intensity curve reflecting the arrival of hyperpolarized pyruvate and its conversion into hyperpolarized lactate. These curves were integrated in time to calculate the total relative amounts of hyperpolarized pyruvate and lactate observed over the course of each experiment, and a normalized measure of lactate was formed by dividing total lactate by the sum of lactate and pyruvate. Animals were also scanned at 4.7T using dedicated 1H anatomic imaging coils (35-mm ID) for better depiction of disease progression.

Results

ATC cell line characterization

Eight previously isolated and described ATC cell lines were used in this study. Genomic screening of 140 mutational hotspots contained within 26 genes (Supplementary Table S1) confirmed previously identified *BRAF V600E* mutations in 4 cell lines (U-HTH83, U-HTH104, 8505C, and SW1726) and identified nonsynonymous mutations in *KIT* (D816H; U-HTH7) and *N-RAS* (Q61R; U-HTH7). With the exception of *BRAF*, no other common genomic alteration was found that would suggest efficacy of currently available targeted therapeutic strategies.

Anaplastic tumors generally display an aggressive histology with both epithelial and mesenchymal features (23–25). Of the 8 ATC cell lines evaluated here, only 1 (U-HTH83) exhibited an epithelial morphology and high expression of E-cadherin (Fig. 1). The remaining 7 cell lines had variable vimentin expression, no E-cadherin expression, and a mesenchymal morphology. Given the shown link between a mesenchymal phenotype and resistance to conventional chemotherapy, these findings were discouraging from a therapeutic perspective and prompted us to expand our investigation to other aspects of ATC tumor cell biology.

Glucose catabolism is required for ATC cell line proliferation and survival

Under normal growth conditions (glucose and glutamine) U-HTH83 and U-HTH74 exhibited the highest proliferative rates (Fig. 2). Cell proliferation was measured under conditions of glucose or glutamine deprivation to identify the primary metabolic substrate for this tumor type. In the absence of glutamine, cell number at the 72-hour time point decreased by between 8% (U-HTH74) to 56% (C643) compared with the control condition. In the absence of glucose, corresponding decreases were larger and ranged from 24% (SW1736) to 92% (U-HTH74). Glucose, but not glutamine, starvation resulted in cell death between 48 and 72 hours (Supplementary Fig. S1). Together these data strongly suggested that, although glutamine

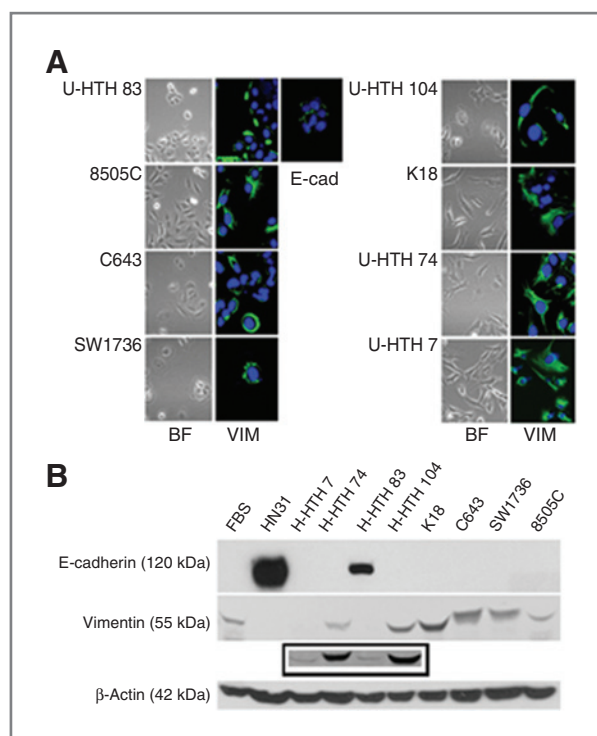


Figure 1. ATC cell lines exhibit predominantly mesenchymal morphology and characteristics. A, ATC cells were imaged using bright-field microscopy and following staining with E-cadherin (1:100) and vimentin (1:100). B, protein lysates were analyzed for expression of E-cadherin (1:1,000) and vimentin (1:1,000) using Western blotting. Control lysates were used from thyroid fibroblasts (FBS) and an epithelial HNSCC cell line (HN31). Note: U-HTH 7 expressed vimentin by Western blotting though at much lower levels compared with the remaining cell lines. Inset contains longer exposure of above film.

is needed for ATC cell proliferation, glucose is the primary nutrient, at least under *in vitro* conditions.

ATC energy levels (ATP) and intracellular potential are driven by the extracellular glucose concentration

Tumor cells can limit DNA damage induced by chemotherapeutic agents and XRT through multiple mechanisms including active efflux, protein binding of toxic compounds, and inactivation of reactive oxygen species (ROS). These mechanisms are energy demanding, the former because of ATP requirements of active transport, the latter 2 because of the need for reducing equivalents to regenerate inactivating proteins such as glutathione (11). As illustrated in Fig. 3, ATC intracellular reducing potential is driven by changes in the extracellular glucose concentration, and not by changes in the glutamine concentration. Although these phenomena occur under *in vitro* conditions, the results suggested that pharmacologic targeting of glycolysis alone could significantly alter ATC intracellular energy stores and reducing potential.

To confirm this hypothesis, we used a competitive inhibitor of glucose, 2-DG, which is taken up through glucose transporters and phosphorylated by hexokinase resulting in a nonmetabolizable derivative. Administration of 2-DG

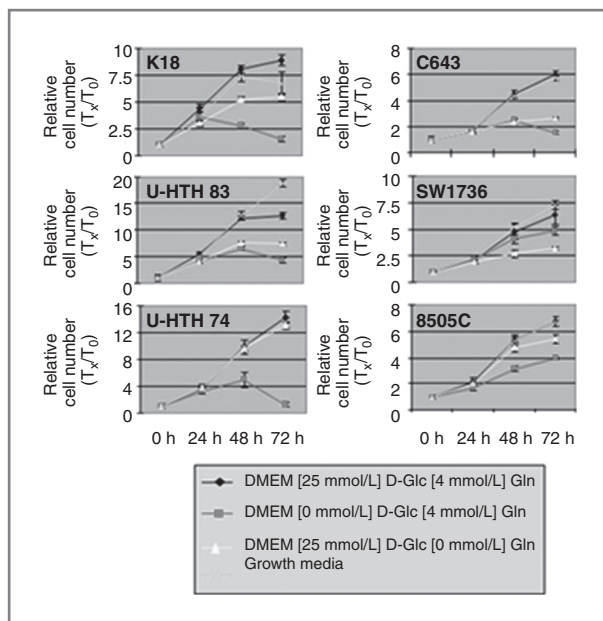


Figure 2. Removal of glucose and glutamine results in decreased ATC cell population growth. Six ATC lines were grown in 96-well plates at 3,000 cells per well under conditions of glucose or glutamine deprivation as well as standard growth media. Total DNA was assayed at indicated time points and used as a surrogate for cell number. Glucose (D-Glc) deprivation markedly reduced cell proliferation as normalized to control for all lines. Glutamine (Gln) dependence was most clearly observed in SW1736, U-HTH83, and C643. Each condition was tested in triplicate and each experiment was conducted at least twice.

decreased both intracellular reducing potential and ATP levels in a dose-dependent manner, beginning at equimolar doses with the extracellular glucose concentration (Fig. 3). On the basis of these data, we next

evaluated the effects of glycolytic inhibition of ATC cell proliferation and survival in the single-agent setting as well as in combination with conventional chemotherapy and XRT.

2-Deoxyglucose potentiates the cytotoxic effects of chemotherapy and XRT

In the single-agent setting, glycolytic inhibition using 2-DG resulted in a cytostatic effect, with IC_{50} values in the single mmol/L range, consistent with our previous experience in other solid tumor types (data not shown; ref. 18). The combination of 2-DG and cisplatin resulted in increased cell cytotoxicity compared with either agent alone (Fig. 4A).

Baseline *in vitro* radiosensitivity varied dramatically among ATC cell lines tested, with C643 as the least and U-HTH 74 as the most sensitive cell lines. The addition of cisplatin or 2-DG potentiated XRT effects with the combination exhibiting an enhanced effect (representative data shown in Fig. 4B). Although the underlying sensitivity of ATC cells to each single agent (2-DG, cisplatin, and XRT) varied, the combination of all or both drugs with XRT resulted universally in significantly greater cell killing effects than either agent alone.

2-DG transiently decreases ATC tumor reducing potential *in vivo*

Previous studies have shown *in vivo* 2-DG potentiation of chemotherapy and radiation effects in various solid tumor types (12, 13). These studies however have had to use supraphysiologic doses administered in a continuous manner to achieve modest therapeutic effects. A short plasma half-life has been thought to contribute to the therapeutic limitations of 2-DG. Until now, however,

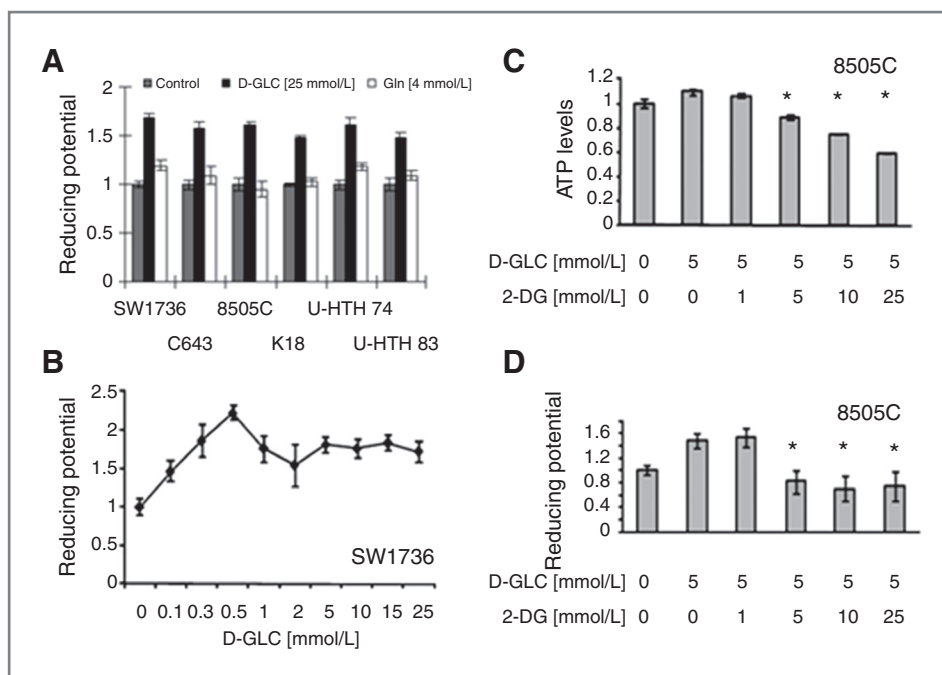


Figure 3. ATC intracellular ATP and reducing potential levels are driven by extracellular glucose. A–D, cells were exposed to various concentrations of glucose or glutamine in the presence or absence of 2-DG for 2 hours. Intracellular ATP levels were assayed using a commercially available kit. Reducing potential was assayed using a modified MTT reaction. *, *P* value less than 0.05 (by Student *t* test) compared with the D-Glc [5 mmol/L] condition. Control condition for panel A represents reducing potential in the absence of both glucose and glutamine. Each condition was tested in triplicate and each experiment was conducted at least twice.

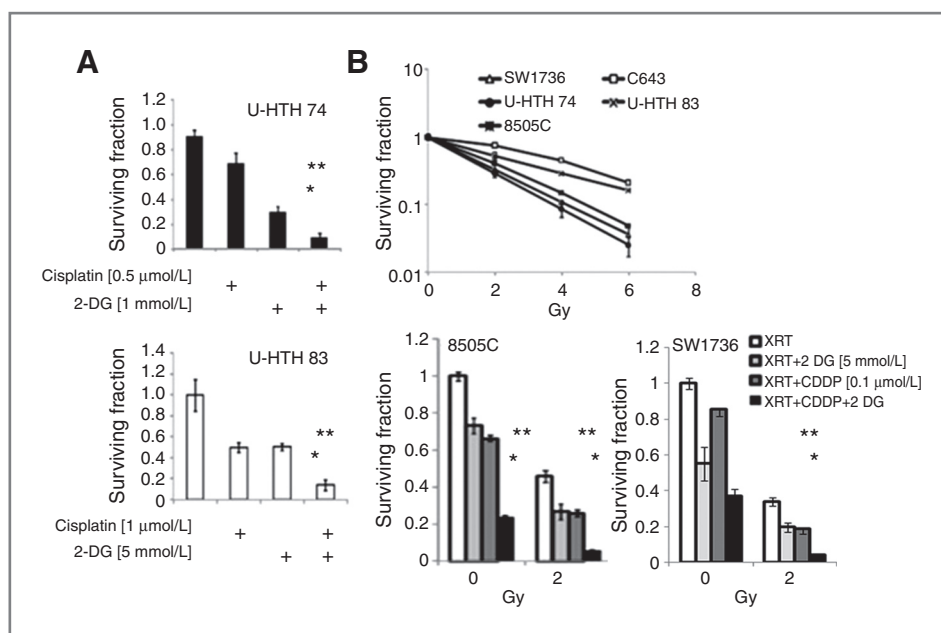


Figure 4. 2-DG can potentiate the cytotoxic effects of cisplatin and XRT. A, ATC cells were exposed to cisplatin and 2-DG for 24 hours followed by a 7- to 10-day recovery period. Data are representative of multiple independent experiments with multiple ATC cell lines. **, *P* value less than 0.05 (by Student *t* test) compared with the 2-DG-treated condition. *, *P* value less than 0.05 compared with the cisplatin-treated condition. B, ATC cell lines were exposed to XRT in the absence or presence of cisplatin (CDDP) and/or 2-DG at the doses indicated. At the end of the experimental time period, colonies were stained and counted and expressed as a fraction of the control condition. **, *P* value less than 0.05 (by Student *t* test) compared with the 2-DG+XRT-treated condition. *, *P* value less than 0.05 compared with the cisplatin+XRT-treated condition. Each condition was tested in triplicate and each experiment was conducted at least twice.

there has been no report of the dynamic effects of 2-DG on *in vivo* tumor metabolism.

Our *in vitro* data suggested that 2-DG would significantly affect the intracellular reducing potential of ATC cells. Because the pyruvate–lactate reaction representing the final step in glycolysis is partially driven by the intracellular reducing potential, we used hyperpolarized (HP) ^{13}C MRI (HP-MRI) using labeled pyruvate to evaluate 2-DG effects on tumor metabolism.

ATC xenografts exhibited rapid growth and aggressive locoregional expansion, with envelopment of critical structures including trachea and esophagus (Fig. 5). Deposition of ^{13}C label from the pyruvate into the lactate pool was observed in dynamic spectra as a growth of signal at the resonance corresponding to C1 of lactate following injection of hyperpolarized pyruvate (Supplementary Fig. S2). A small increase in lactate signal was noted across the experimental time period (Fig. 6A), consistent with the measured increase in tumor size. Following administration of 2-DG, the net conversion of hyperpolarized pyruvate into lactate was lower in treated tumors ($n = 3$) than in control tumors ($n = 4$) at 2-hour posttreatment ($P = 0.0504$; Fig. 6B and C). This effect was not observed at 24 hours posttreatment, with lactate signal varying quite significantly in treated tumors at this time point (data not shown). A second measurement at week 2 showed a similar trend (data not shown), although it is important to note that the second measurement was

obtained in tumors that were no longer naive to 2-DG exposure.

Discussion

Despite its low prevalence, anaplastic thyroid cancer remains one of the most difficult cancers to treat. The high rate of locoregional invasion and distant metastasis makes advanced disease at time of presentation common and limits therapeutic options. The use of multimodality treatment strategies has failed to substantially improve clinical outcomes to date (2). One explanation for this failure is the presence of extensive microscopic disease at the time of presentation, which fails to be addressed either surgically or with XRT. Novel therapeutic agents must be identified to improve treatment effectiveness and reduce the morbidity and mortality associated with ATC.

Multiple conventional and targeted therapeutic agents have been used in the preclinical setting (cell lines and mouse xenografts) to variable effect (2, 20, 26–28). In clinical studies, conventional agents such as cisplatin or doxorubicin have shown some effect with respect to disease progression but failed to significantly alter overall survival. Targeted agents such as gefitinib and sorafenib have similarly modest effects when combined with XRT and conventional chemotherapy (1–3, 26, 28, 29). We analyzed 26 commonly mutated genes to identify putative

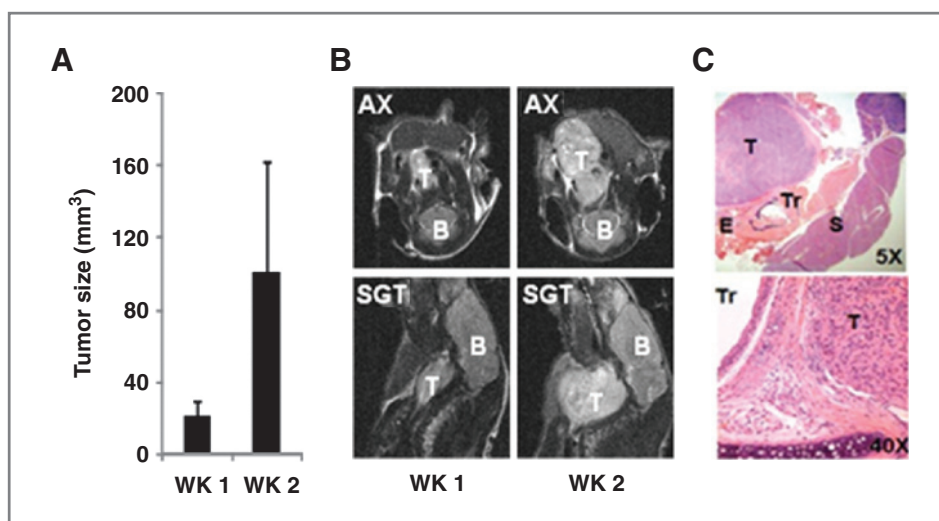


Figure 5. Real-time imaging of ATC xenografts. A, tumor volume data indicating increasing tumor size during the experimental period and B, representative axial (AX) and sagittal (SGT) 4.7T MRI images (B, brain stem/brain; T, tumor). C, representative H&E images of tumor architecture indicating relationship with adjacent structures and invasion (Tr, trachea; E, esophagus; T, tumor; S, submandibular gland).

targets for existing molecular agents. With the exception of the *BRAF V600E* mutation, no other mutational events were common among the 8 cell lines tested. In addition, the majority of cell lines tested exhibited a mesenchymal phenotype known to correlate with resistance to conventional chemotherapeutic agents. In light of these data, we sought to evaluate an alternative strategy that has received increasing attention in recent years: antimetabolic targeting.

Under *in vitro* growth conditions, ATC cell lines require both glucose and glutamine for maximal proliferation, but glucose is essential for maintenance of intracellular ATP, reducing equivalents and survival. Inhibition of glucose catabolism using 2-DG decreased energy levels and improved the cytotoxicity of cisplatin and XRT. Other studies have shown that such effects can be reproduced in preclinical animal models, but only using prolonged administration of supraphysiologic doses of 2-DG (6, 12). Because these treatment regimens cannot be used in the patient population, no clinical applications for 2-DG have been identified despite 30 years of investigation.

One major limitation of 2-DG is its presumed poor *in vivo* pharmacodynamic profile. Extrapolation from plasma kinetic data has suggested that 2-DG effects *in vivo* are short lasting and preclude persistent metabolic inhibition of tumors (13). To date, it has not been possible to directly measure the magnitude and duration of 2-DG effects on tumor metabolism *in vivo*. This is largely because the primary metabolic imaging modality currently available ¹⁸fluoro-2-DG-PET is incompatible with 2-DG treatment.

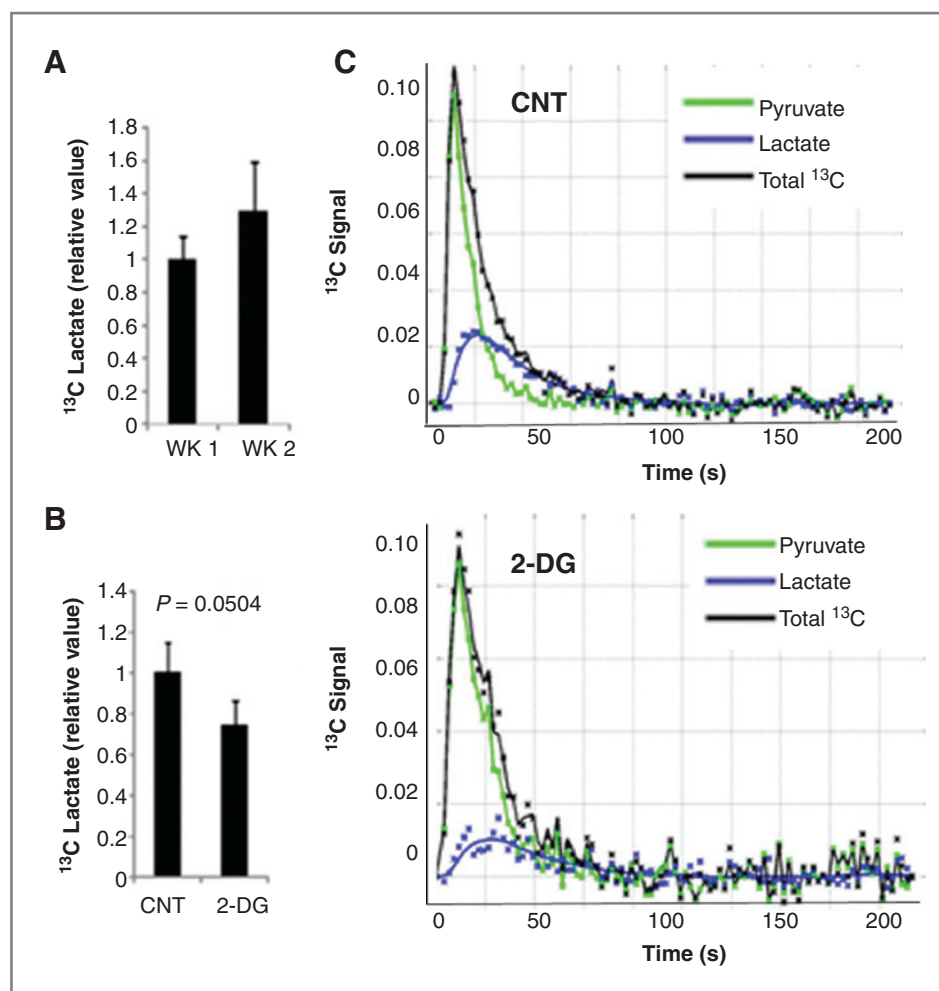
To evaluate the effects of 2-DG on ATC tumor metabolism, we used real-time MRI in the context of an orthotopic xenograft murine model. HP-MRI has been used in recent years to improve disease staging and to guide therapeutic interventions (30). Pyruvate lactate conversion represents the ultimate step of aerobic glycolysis. This reaction is controlled in part by the availability of

reducing equivalents. Changes in the rate of conversion indirectly reflect the reducing potential of tumors. This is important for 2 reasons. First, reducing equivalents are essential for cellular energy and biomass production. Second, reducing equivalents are used by cells to neutralize ROS and prevent DNA damage. Because ROS are the primary mechanism by which XRT induces cell death, the reducing potential of tumors is not only important for tumor growth but also essential for tumor radiosensitivity.

Consistent with its *in vitro* effects, 2-DG administration resulted in a significant decrease in ATC xenograft reducing potential as shown by decreased HP-MRI signal. Importantly however, the magnitude of the decrease was limited (~30%) and short lived (<24 hours). Together, these data showed experimentally for the first time that (i) 2-DG does in fact inhibit solid tumor metabolism, (ii) the magnitude of this inhibition is small, and (iii) its effective duration is limited. In light of these results, there is a clear need for improved chemistry of antiglycolytic agents designed to improve *in vivo* effective half-life. There exist 2-DG derivatives whose altered chemistry results in increased inhibition of hexokinase activity (7). To address the short *in vivo* half-life of 2-DG, prodrugs are being described with improved pharmacodynamics (9). It is likely that these developments will advance glycolytic inhibition from an *in vitro* phenomenon to a clinical reality in the next few years.

On the basis of our initial data, we believe that HP-MRI is a promising method to evaluate the pharmacodynamic profile of next generation antiglycolytic agents. Integration of this imaging platform with real-time capability will be essential to the development of an iterative process of drug design and optimization which combines *in vitro* biochemical assays with preclinical animal models of disease. Ongoing studies in our laboratory are aimed at establishing the validity of this paradigm in the context of ATC.

Figure 6. 2-DG suppresses HP-MRI signal in ATC xenografts. **A**, normalized levels of hyperpolarized lactate (to total hyperpolarized carbon) from pyruvate–lactate conversion across the 2-week experimental period showing increased net lactate signal associated with tumor growth. **B**, HP-lactate signal in tumor was decreased at 2 hours following administration of 2-DG (500 mg/kg i.p.) in week 1 (control tumors = 4, treated tumors = 3). **C**, representative tracings of ^{13}C signal and pyruvate–lactate conversion in control (CNT) and 2-DG (500 mg/kg) treated tumors at 2-hour posttreatment (2-DG).



Conclusions

ATC cells possess few targetable biologic pathways and exhibit a mesenchymal phenotype associated with resistance to conventional agents. Generalized dependence on glucose catabolism makes them susceptible to the effects of antiglycolytic agents. To translate the effects observed *in vitro* however, newer antiglycolytic compounds with increased effective half-life and potency will be required. The use of HP-MRI represents an essential tool for monitoring the *in vivo* effectiveness of such novel therapeutic agents and can greatly aid in their design and clinical testing in this and other solid tumors.

Disclosure of Potential Conflicts of Interest

No potential conflicts of interest were disclosed.

Authors' Contributions

Conception and design: V.C. Sandulache, H.D. Skinner, T.J. Ow, J.A. Bankson, S.Y. Lai

Development of methodology: V.C. Sandulache, H.D. Skinner, J.A. Bankson, S.Y. Lai

Acquisition of data (provided animals, acquired and managed patients, provided facilities, etc.): V.C. Sandulache, H.D. Skinner, Y. Wang, Y. Chen, T.J. Ow, J.A. Bankson, S.Y. Lai

Analysis and interpretation of data (e.g., statistical analysis, biostatistics, computational analysis): V.C. Sandulache, H.D. Skinner, T.J. Ow, J.A. Bankson, S.Y. Lai

Writing, review, and/or revision of the manuscript: V.C. Sandulache, H.D. Skinner, C.T. Dodge, T.J. Ow, J.A. Bankson, J.N. Myers, S.Y. Lai

Administrative, technical, or material support (i.e., reporting or organizing data, constructing databases): V.C. Sandulache, C.T. Dodge, J.A. Bankson

Study supervision: J.A. Bankson, J.N. Myers, S.Y. Lai

Acknowledgments

The authors thank Dr. Matthew Merritt, PhD for his review of and suggestions for the manuscript. The content is solely the responsibility of the authors and does not necessarily represent the official views of the National Cancer Institute or the NIH.

Grant Support

This research is supported in part by the NIH through National Research Science Award Research Training Grant (NCI) T32 CA060374 (V.C. Sandulache), NIH Mentored Career Development Award K08 DE18061 (S.Y. Lai), the NIH Cancer Center Support grant P30 CA016672 (MD Anderson Cancer Center) and the NCI Small Animal Imaging Resource Program U24 CA126577 (MD Anderson Cancer Center).

The costs of publication of this article were defrayed in part by the payment of page charges. This article must therefore be hereby marked *advertisement* in accordance with 18 U.S.C. Section 1734 solely to indicate this fact.

Received January 16, 2012; revised March 23, 2012; accepted March 29, 2012; published OnlineFirst May 9, 2012.

References

- Bhatia A, Rao A, Ang KK, Garden AS, Morrison WH, Rosenthal DI, et al. Anaplastic thyroid cancer: Clinical outcomes with conformal radiotherapy. *Head Neck* 2010;32:829–36.
- Smallridge RC, Copland JA. Anaplastic thyroid carcinoma: pathogenesis and emerging therapies. *Clin Oncol (R Coll Radiol)* 2010;22:486–97.
- Tsimberidou AM, Vaklavas C, Wen S, Hong D, Wheeler J, Ng C, et al. Phase I clinical trials in 56 patients with thyroid cancer: the M. D. Anderson Cancer Center experience. *J Clin Endocrinol Metab* 2009;94:4423–32.
- Warburg O. On the origin of cancer cells. *Science* 1956;123:309–14.
- Vander Heiden MG, Cantley LC, Thompson CB. Understanding the Warburg effect: the metabolic requirements of cell proliferation. *Science* 2009;324:1029–33.
- Maschek G, Savaraj N, Priebe W, Braunschweiger P, Hamilton K, Tidmarsh GF, et al. 2-Deoxy-D-glucose increases the efficacy of adriamycin and paclitaxel in human osteosarcoma and non-small cell lung cancers *in vivo*. *Cancer Res* 2004;64:31–4.
- Lampidis TJ, Kurtoglu M, Maher JC, Liu H, Krishan A, Sheft V, et al. Efficacy of 2-halogen substituted D-glucose analogs in blocking glycolysis and killing "hypoxic tumor cells". *Cancer Chemother Pharmacol* 2006;58:725–34.
- Mohanti BK, Rath GK, Anantha N, Kannan V, Das BS, Chandramouli BA, et al. Improving cancer radiotherapy with 2-deoxy-D-glucose: phase I/II clinical trials on human cerebral gliomas. *Int J Radiat Oncol Biol Phys* 1996;35:103–11.
- Priebe W, Skora S, Conrad CA, Madden T. Blocking glycolysis with 2-deoxy-D-glucose prodrugs to target brain tumors: a novel concept. *Molecular Cancer Therapeutics* 2009;8.
- Sandulache VC, Ow TJ, Pickering CR, Frederick MJ, Zhou G, Fokt I, et al. Glucose, not glutamine, is the dominant energy source required for proliferation and survival of head and neck squamous carcinoma cells. *Cancer* 2011;117:2926–38.
- Simons AL, Ahmad IM, Mattson DM, Dornfeld KJ, Spitz DR. 2-Deoxy-D-glucose combined with cisplatin enhances cytotoxicity via metabolic oxidative stress in human head and neck cancer cells. *Cancer Res* 2007;67:3364–70.
- Simons AL, Fath MA, Mattson DM, Smith BJ, Walsh SA, Graham MM, et al. Enhanced response of human head and neck cancer xenograft tumors to cisplatin combined with 2-deoxy-D-glucose correlates with increased 18F-FDG uptake as determined by PET imaging. *Int J Radiat Oncol Biol Phys* 2007;69:1222–30.
- Singh D, Banerji AK, Dwarakanath BS, Tripathi RP, Gupta JP, Mathew TL, et al. Optimizing cancer radiotherapy with 2-deoxy-d-glucose dose escalation studies in patients with glioblastoma multiforme. *Strahlenther Onkol* 2005;181:507–14.
- Kim YW, Do IG, Park YK. Expression of the GLUT1 glucose transporter, p63 and p53 in thyroid carcinomas. *Pathol Res Pract* 2006;202:759–65.
- Schonberger J, Ruschoff J, Grimm D, Marienhagen J, Rummele P, Meyringer R, et al. Glucose transporter 1 gene expression is related to thyroid neoplasms with an unfavorable prognosis: an immunohistochemical study. *Thyroid* 2002;12:747–54.
- Zhao M, Sano D, Pickering CR, Jasser SA, Henderson YC, Clayman GL, et al. Assembly and initial characterization of a panel of 85 genomically validated cell lines from diverse head and neck tumor sites. *Clin Cancer Res* 2011;17:7248–64.
- Sternke-Hale K, Gonzalez-Angulo AM, Lluch A, Neve RM, Kuo WL, Davies M, et al. An integrative genomic and proteomic analysis of PIK3CA, PTEN, and AKT mutations in breast cancer. *Cancer Res* 2008;68:6084–91.
- Sandulache VC, Ow TJ, Pickering CR, Frederick MJ, Zhou G, Fokt I, et al. Glucose, not glutamine, is the dominant energy source required for proliferation and survival of head and neck squamous carcinoma cells. *Cancer* 2011;117:2926–38.
- Sandulache VC, Skinner HD, Ow TJ, Zhang A, Xia X, Luchak JM, et al. Individualizing antimetabolic treatment strategies for head and neck squamous cell carcinoma based on TP53 mutational status. *Cancer* 2012;118:711–21.
- Gule MK, Chen Y, Sano D, Frederick MJ, Zhou G, Zhao M, et al. Targeted therapy of VEGFR2 and EGFR significantly inhibits growth of anaplastic thyroid cancer in an orthotopic murine model. *Clin Cancer Res* 2011;17:2281–91.
- Golman K, in 't Zandt R, Thaning M. Real-time metabolic imaging. *Proc Natl Acad Sci U S A* 2006;103:11270–5.
- Ardenjaer-Larsen JH, Fridlund B, Gram A, Hansson G, Hansson L, Lerche MH, et al. Increase in signal-to-noise ratio of > 10,000 times in liquid-state NMR. *Proc Natl Acad Sci U S A* 2003;100:10158–63.
- Brabant G, Hoang-Vu C, Cetin Y, Dralle H, Scheumann G, Molne J, et al. E-cadherin: a differentiation marker in thyroid malignancies. *Cancer Res* 1993;53:4987–93.
- Hoffmann S, Maschuw K, Hassan I, Reckzeh B, Wunderlich A, Lingelbach S, et al. Differential pattern of integrin receptor expression in differentiated and anaplastic thyroid cancer cell lines. *Thyroid* 2005;15:1011–20.
- Husmark J, Heldin NE, Nilsson M. N-cadherin-mediated adhesion and aberrant catenin expression in anaplastic thyroid-carcinoma cell lines. *Int J Cancer* 1999;83:692–9.
- Kim S, Prichard CN, Younes MN, Yazici YD, Jasser SA, Bekele BN, et al. Cetuximab and irinotecan interact synergistically to inhibit the growth of orthotopic anaplastic thyroid carcinoma xenografts in nude mice. *Clin Cancer Res* 2006;12:600–7.
- Liu D, Xing M. Potent inhibition of thyroid cancer cells by the MEK inhibitor PD0325901 and its potentiation by suppression of the PI3K and NF-kappaB pathways. *Thyroid* 2008;18:853–64.
- Voigt W, Kegel T, Weiss M, Mueller T, Simon H, Schmoll HJ. Potential activity of paclitaxel, vinorelbine and gemcitabine in anaplastic thyroid carcinoma. *J Cancer Res Clin Oncol* 2005;131:585–90.
- Voigt W, Bulankin A, Muller T, Schoeber C, Grothey A, Hoang-Vu C, et al. Schedule-dependent antagonism of gemcitabine and cisplatin in human anaplastic thyroid cancer cell lines. *Clin Cancer Res* 2000;6:2087–93.
- Kurhanewicz J, Vigneron DB, Brindle K, Chekmenev EY, Comment A, Cunningham CH, et al. Analysis of cancer metabolism by imaging hyperpolarized nuclei: prospects for translation to clinical research. *Neoplasia* 2011;13:81–97.

Molecular Cancer Therapeutics

Glycolytic Inhibition Alters Anaplastic Thyroid Carcinoma Tumor Metabolism and Improves Response to Conventional Chemotherapy and Radiation

Vlad C. Sandulache, Heath D. Skinner, Yuan Wang, et al.

Mol Cancer Ther 2012;11:1373-1380. Published OnlineFirst May 9, 2012.

Updated version Access the most recent version of this article at:
[doi:10.1158/1535-7163.MCT-12-0041](https://doi.org/10.1158/1535-7163.MCT-12-0041)

Supplementary Material Access the most recent supplemental material at:
<http://mct.aacrjournals.org/content/suppl/2012/04/17/1535-7163.MCT-12-0041.DC1>

Cited articles This article cites 29 articles, 12 of which you can access for free at:
<http://mct.aacrjournals.org/content/11/6/1373.full#ref-list-1>

Citing articles This article has been cited by 5 HighWire-hosted articles. Access the articles at:
<http://mct.aacrjournals.org/content/11/6/1373.full#related-urls>

E-mail alerts [Sign up to receive free email-alerts](#) related to this article or journal.

Reprints and Subscriptions To order reprints of this article or to subscribe to the journal, contact the AACR Publications Department at pubs@aacr.org.

Permissions To request permission to re-use all or part of this article, use this link
<http://mct.aacrjournals.org/content/11/6/1373>.
Click on "Request Permissions" which will take you to the Copyright Clearance Center's (CCC) Rightslink site.